

See discussions, stats, and author profiles for this publication at: <https://www.researchgate.net/publication/49655508>

The Tightly Bound Calcium of MauG Is Required for Tryptophan Tryptophylquinone Cofactor Biosynthesis

ARTICLE *in* BIOCHEMISTRY · DECEMBER 2010

Impact Factor: 3.02 · DOI: 10.1021/bi101819m · Source: PubMed

CITATIONS

13

READS

24

8 AUTHORS, INCLUDING:



Sooim Shin

University of Central Florida

19 PUBLICATIONS 156 CITATIONS

[SEE PROFILE](#)



Manliang Feng

Tougaloo College

20 PUBLICATIONS 430 CITATIONS

[SEE PROFILE](#)



Aimin Liu

Georgia State University

79 PUBLICATIONS 1,277 CITATIONS

[SEE PROFILE](#)



Victor L Davidson

University of Central Florida

219 PUBLICATIONS 5,294 CITATIONS

[SEE PROFILE](#)

Published in final edited form as:

Biochemistry. 2011 January 11; 50(1): 144–150. doi:10.1021/bi101819m.

The tightly bound calcium of MauG is required for tryptophan tryptophylquinone cofactor biosynthesis

Sooim Shin¹, Manliang Feng¹, Yan Chen², Lyndal M. R. Jensen³, Hiroyasu Tachikawa⁴, Carrie M. Wilmot³, Aimin Liu², and Victor L. Davidson¹

¹ Department of Biochemistry, University of Mississippi Medical Center, Jackson, MS 39216

² Department of Chemistry, Georgia State University, Atlanta, GA, 30302

³ Department of Biochemistry, Molecular Biology and Biophysics, University of Minnesota, 321 Church St. SE, Minneapolis, MN 55455

⁴ Department of Chemistry, Jackson State University, Jackson, MS 39217

Abstract

The diheme enzyme MauG catalyzes a six-electron oxidation required for posttranslational modification of a precursor of methylamine dehydrogenase (preMADH) to complete the biosynthesis of its protein-derived tryptophan tryptophylquinone (TTQ) cofactor. The crystal structure of the MauG-preMADH complex revealed the presence of a Ca^{2+} in proximity to the two hemes [Jensen, L.M.R., Sanishvili, R., Davidson, V.L. & Wilmot, C.M. (2010) *Science* 327, 1392–1394]. This Ca^{2+} did not readily dissociate; however after extensive treatment with EGTA or EDTA MauG was no longer able to catalyze TTQ biosynthesis and exhibited altered absorption and resonance Raman spectra. The changes in spectral features are consistent with Ca^{2+} -dependent changes in heme spin-state and conformation. Addition of H_2O_2 to the Ca^{2+} -depleted MauG did not yield spectral changes characteristic of formation of the *bis*-Fe(IV) state which is stabilized in native MauG. After addition of Ca^{2+} to the Ca^{2+} -depleted MauG, full TTQ biosynthesis activity and reactivity towards H_2O_2 was restored, and the spectral properties returned to those of native MauG. Kinetic and equilibrium studies of Ca^{2+} binding to Ca^{2+} -depleted MauG indicated a two-step mechanism. Ca^{2+} initially reversibly binds to Ca^{2+} -depleted MauG ($K_d = 22.4 \mu\text{M}$) and is followed by a relatively slow ($k = 1.4 \times 10^{-3} \text{ s}^{-1}$) but highly favorable ($K_{eq} = 4.2$) conformational change, yielding an apparent equilibrium $K_{d,eq}$ value of $5.3 \mu\text{M}$. The circular dichroism spectra of native and Ca^{2+} -depleted MauG were essentially the same, consistent with Ca^{2+} -induced conformational changes involving domain or loop movements rather than general unfolding or alteration of secondary structure. These results are discussed in the context of the structures of MauG and heme-containing peroxidases.

Calcium participates in a variety of important biological functions, many of which are accomplished through interaction with proteins. Ca^{2+} binding allows muscle contraction through conformational transitions in troponin C (1). The calcium binding protein calmodulin regulates a number of different protein targets, thereby affecting many different cellular functions (2). Ca^{2+} is required for the activity of enzymes such as phospholipase A_2 (3). Ca^{2+} has also been detected in heme-containing peroxidases of plants, fungi, bacteria and animals, including canine myeloperoxidase (4), horseradish peroxidase (5,6), cationic peanut peroxidase (7), manganese peroxidase (8), lignin peroxidase (9), and bacterial diheme cytochrome *c* peroxidase (BCCP)1 (10). In general, Ca^{2+} has been proposed to

maintain a heme conformation and heme pocket structure associated with high catalytic activities for these peroxidases.

Bound Ca^{2+} has also been found in the crystal structure of the diheme enzyme MauG from *Paracoccus denitrificans* (11) (Figure 1). MauG exhibits approximately 30% sequence homology to BCCPs (10,12) and the crystal structures of MauG and various BCCPs reveal that the orientation of the Ca^{2+} and two hemes is essentially identical in the two classes of proteins (10,11,13). Despite this structural similarity, BCCPs and MauG exhibit significant differences in catalytic and redox behavior (14,15). MauG catalyzes the final steps in the biosynthesis of the protein-derived cofactor (16), tryptophan tryptophylquinone (TTQ) (17) in methylamine dehydrogenase (MADH). MauG catalyzes a six-electron oxidation of a precursor protein (preMADH) containing monohydroxylated $\beta\text{Trp}57$ (Scheme 1). During this process a second oxygen atom is inserted into the indole ring of $\beta\text{Trp}57$, $\beta\text{Trp}57$ is covalently crosslinked to $\beta\text{Trp}108$ and the quinol species is oxidized to the quinone. These reactions proceed via a high valent *bis*-Fe(IV) redox state of MauG that may be generated by reaction of diferrous MauG with molecular oxygen or reaction of diferric MauG with H_2O_2 (18).

The role of Ca^{2+} in BCCPs has been extensively studied and it has been found to be essential for activity (10). For most BCCPs the as-isolated enzyme is in an inactive diferric state in which the H_2O_2 -binding heme is six-coordinate with His-His axial ligation (19). The reduction of the other heme in BCCP, which is six-coordinate with His-Met ligation, generates a mixed-valence state that triggers a Ca^{2+} -dependent conformational change in which the distal His ligand of the H_2O_2 -binding heme is replaced by water (20,21). This activated form of the enzyme then proceeds through its normal reaction cycle. Relaxation back to the fully oxidized inactive state only occurs when insufficient reductant is present, and therefore the diferric form is not considered part of the catalytic cycle of the BCCPs. MauG also has Ca^{2+} bound with identical ligation to that of BCCP, but in this case the diferric enzyme is active, and there is no evidence for the mixed-valence state that is central in the reaction cycle of BCCP. Thus while structurally conserved, the role of Ca^{2+} in MauG is clearly different from that in BCCP.

In this study we report methods to reversibly remove Ca^{2+} from MauG and reconstitute the Ca^{2+} -depleted MauG with Ca^{2+} . This allowed the characterization of the effects of Ca^{2+} on the physical and catalytic properties of MauG. The Ca^{2+} -depleted MauG is inactive in TTQ biosynthesis and exhibits altered spectral properties. The results reveal Ca^{2+} -dependent changes in heme spin-state and heme conformation. These changes are reversible, as after incubation of Ca^{2+} -depleted MauG with Ca^{2+} the native spectral properties and activity are regained. The reconstitution with Ca^{2+} is shown to proceed via a two-step mechanism of reversible binding followed by a conformational change. MauG uses H_2O_2 to catalyze posttranslational modifications of a protein substrate but it does not function primarily as a peroxidase. Despite this different reactivity, MauG shares the common feature of a bound Ca^{2+} in proximity to the heme(s) that is seen in *b*-type heme peroxidases and *c*-type diheme peroxidases. The effects of removal of Ca^{2+} from MauG on its spectroscopic and catalytic properties, and the mechanism of Ca^{2+} binding to Ca^{2+} -depleted MauG, are discussed and compared with studies of the roles of Ca^{2+} in peroxidases.

¹Abbreviations: MADH, methylamine dehydrogenase; TTQ, tryptophan tryptophylquinone; preMADH, the biosynthetic precursor protein of MADH with incompletely synthesized TTQ; BCCP, bacterial diheme cytochrome *c* peroxidase; ET, electron transfer; *bis*-Fe(IV) MauG, redox state of MauG with one heme as Fe(IV)=O and the other as Fe(IV); CD, circular dichroism.

Experimental procedures

Protein purification and preparation

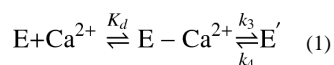
Methods for the expression and purification of MADH (22), preMADH (23), and MauG (12) were as described previously. Concentrations of these proteins were calculated using the following extinction coefficients: diferric MauG ($\epsilon_{406} = 309,000 \text{ M}^{-1}\text{cm}^{-1}$), quinone MADH ($\epsilon_{440} = 26,200 \text{ M}^{-1}\text{cm}^{-1}$) and quinol MADH ($\epsilon_{330} = 56,400 \text{ M}^{-1}\text{cm}^{-1}$). Ca^{2+} -depleted MauG was prepared by incubation of native MauG with either 0.01 M EDTA-disodium salt or EGTA in 0.01 M potassium phosphate buffer, pH 7.5, for 15 hours at 4 °C. The chelator was removed and the buffer was exchanged to 0.05 M Tris-HCl, pH 7.5 by centrifugation. Ca^{2+} -reconstituted MauG was prepared by incubation of Ca^{2+} -depleted MauG with 0.01 M CaCl_2 in 0.05 M Tris-HCl, pH 7.5. Reduction and oxidation of MauG proteins were performed anaerobically using sodium dithionite and potassium ferricyanide, respectively.

Spectrophotometric assay of Ca^{2+} -depleted MauG activity

The activity of Ca^{2+} -depleted MauG was assayed in three different reactions; two involving TTQ biosynthesis and one involving only electron transfer (Scheme 1). Two steady-state spectrophotometric assays of MauG-dependent TTQ biosynthesis using either preMADH (14) or quinol MADH (24) as the substrate were performed as described previously using H_2O_2 as the source of oxidizing equivalents. The single-turnover kinetics of the reaction of diferric Ca^{2+} -depleted MauG with quinone MADH was also studied as described previously for native MauG (24).

Kinetic and equilibrium analysis of Ca^{2+} binding to Ca^{2+} -depleted MauG

Transient kinetic experiments of Ca^{2+} binding to Ca^{2+} -depleted MauG were performed using a Shimadzu Multispec-1501 spectrophotometer. A fixed concentration of 3 μM Ca^{2+} -depleted MauG was mixed with varied concentrations of CaCl_2 solution. The reaction was monitored by the rate of the spectral change corresponding to the return to the spectrum of diferric native MauG. Data were analyzed as described above using eqs 1 and 2 where E is the inactive Ca^{2+} -depleted MauG, and E' is the active Ca^{2+} -reconstituted MauG.



$$k_{obs} = k_3[\text{Ca}^{2+}] / ([\text{Ca}^{2+}] + K_d) + k_4 \quad (2)$$

The equilibrium binding of Ca^{2+} to Ca^{2+} -depleted MauG was also analyzed. CaCl_2 was added to Ca^{2+} -depleted MauG in increasing concentrations and the magnitude of the Ca^{2+} -induced spectral change was recorded after the system had reached equilibrium. These data were analyzed using eq 3 where Y is the absorbance increase at 370 nm, and $K_{d,eq}$ is the apparent K_d value obtained from the equilibrium measurements.

$$Y = Y_{max}[\text{Ca}^{2+}] / (K_{d,eq} + [\text{Ca}^{2+}]) \quad (3)$$

Resonance Raman spectroscopy

Resonance Raman spectra of MauG samples were recorded using a Raman spectrometer consisting of a Spex model 1877 triple spectrograph and a CCD detector as reported

previously (15). A 406.7 nm line from an argon-krypton ion laser (Spectra-Physics BeamLok model 2080-KV) was used as the excitation source, and the Raman signal was collected in a 120° geometry. The laser power was adjusted to ~5 mW at the sample. Each spectrum was recorded with a 60 s accumulation time, and 10 repetitively measured spectra were averaged to improve the quality of the final spectrum. The wavenumbers of the Raman bands in the spectra of the samples were calibrated using the spectrum of cyclohexane as a standard. Samples contained 0.15 mM protein in 0.05 M Tris-HCl, pH 7.5, and spectra were recorded at 25 °C.

Circular dichroism (CD) spectroscopy

The CD spectra (190–250 nm) of native and Ca²⁺-depleted MauG were acquired on a JASCO J-810 spectropolarimeter (JASCO, Easton, MD, USA) at ambient temperature. In each measurement, a MauG sample (7 μM) was placed in a 1 mm path length quartz cell in 0.05 M potassium phosphate, pH 7.5. All spectra were the average of at least 10 scans with a scan rate of 50 nm·min⁻¹. The spectra were converted to the mean residue molar ellipticity θ_λ according to eq 4, where θ_{obs} is the average of measured ellipticity at λ nm, C is the molar concentration, L is the light path (cm), and N is the number of amino acids in the protein sequence.

$$\theta_\lambda = \frac{\theta_{obs}}{C \cdot L \cdot N} \quad (4)$$

Results

Effects of Ca²⁺ on the visible absorption spectrum of MauG

Comparison of the absorption spectra of the diferric native and diferric Ca²⁺-depleted MauG (Figure 2A) reveals that the removal of Ca²⁺ results in a 4 nm red-shift of the absorption maxima of the Soret peak and a narrowing of the peak width. In contrast, the absorption spectra of the diferrous native and diferrous Ca²⁺-depleted MauG (Figure 2B) reveals that the positions of the α , β and Soret peaks are very similar, although a slight narrowing of the Soret peak is observed after removal of Ca²⁺. After reconstitution of Ca²⁺-depleted MauG with Ca²⁺ the spectra of both diferric and diferrous Ca²⁺-reconstituted MauG were essentially identical to the corresponding native MauG spectra (not shown).

Addition of H₂O₂ to native MauG results in formation of a relatively stable *bis*-Fe(IV) redox state which exhibits a decrease in the intensity of the Soret peak and a 2 nm red-shift of the absorption maxima. This *bis*-Fe(IV) species slowly spontaneously decays back to the diferric state over several minutes (18,25). When H₂O₂ was added to Ca²⁺-depleted MauG, a decrease in the intensity of the Soret peak was observed without an accompanying red-shift (Figure 3). In contrast to native MauG this spectral change did not spontaneously return to the initial spectrum, but instead the intensity of the Soret peak continued to slowly decrease over several minutes. Thus, there is no evidence that Ca²⁺-depleted MauG is able to stabilize the *bis*-Fe(IV) redox state. When this experiment was repeated with Ca²⁺-reconstituted MauG the spectral changes and rate of spontaneous decay back to the diferric state were identical to those of native MauG (not shown).

Effects of Ca²⁺ on the resonance Raman spectrum of MauG

Comparison of the resonance Raman spectra of the diferric native MauG and Ca²⁺-depleted MauG revealed that the frequencies of several of the vibration modes are Ca²⁺-dependent. The high frequency region of the spectra (Figure 4A) contains several marker bands that are

sensitive to oxidation state, spin state and the conformation of the heme macrocycle (26–28). The assignment of marker bands is based on the work of Spiro and coworkers (26). The oxidation state marker band (ν_4) is centered at 1374 cm^{-1} in both spectra indicating the presence of ferric state hemes. Native MauG contains a five-coordinate His ligated high-spin heme and a six-coordinate His-Tyr ligated low-spin heme (11). The native MauG spectrum contains ν_2 bands at 1571 (high-spin) and 1587 cm^{-1} (low-spin), and ν_3 bands at 1478 (high-spin) and 1501 cm^{-1} (low-spin). In the spectrum of Ca^{2+} -depleted MauG, only low spin hemes are present, as evidenced by the loss of the high-spin marker bands at 1571 and 1478 cm^{-1} . The ν_{10} band in Ca^{2+} -depleted MauG has also shifted to higher frequency relative to native MauG indicating a more planar heme macrocycle (28, 29).

The low frequency regions of the spectra (Figure 4B) also show Ca^{2+} -dependent changes. These bands originate from the in-plane and out-of-plane deformation modes of the porphyrin ring as well as the vibration modes from the heme substituents (27). Although there is considerable overlap of the bands in this region, frequency changes are clearly discernible. One of the major changes is to the δ ($\text{C}_\beta\text{C}_\alpha\text{S}$) mode, which shifts from 393 cm^{-1} in native MauG to 408 cm^{-1} in Ca^{2+} -depleted MauG. The vibration mode from the thioether bridge ($\nu(\text{C-S})$) which overlaps the ν_7 mode also shifts from 694 cm^{-1} in native MauG to 691 cm^{-1} in Ca^{2+} -depleted MauG. These changes suggest conformational changes impacting the thioether bridges which may originate from Ca^{2+} -dependent conformational changes of the protein backbone.

Effect of Ca^{2+} on MauG-dependent TTQ biosynthesis activity and interprotein electron transfer reactivity

The activity of Ca^{2+} -depleted MauG was assayed in three different reactions, two involving TTQ biosynthesis and one involving only electron transfer (Scheme 1). Using spectroscopic steady-state assays in which native MauG has been shown to catalyze TTQ biosynthesis with either preMADH or quinol MADH as a substrate (24,25), no detectable TTQ biosynthesis activity was observed for Ca^{2+} -depleted MauG. After re-incorporation of Ca^{2+} , the reconstituted MauG exhibited normal TTQ biosynthesis activity with both substrates. The k_{cat} values for the reaction of native and Ca^{2+} -reconstituted MauG with quinol MADH were $4.4 \pm 0.1\text{ s}^{-1}$ and $4.3 \pm 0.1\text{ s}^{-1}$, respectively. The k_{cat} values for the reaction of native and Ca^{2+} -reconstituted MauG with preMADH were $0.10 \pm 0.01\text{ s}^{-1}$ and $0.09 \pm 0.01\text{ s}^{-1}$, respectively.

Native MauG also exhibits activity in an electron transfer reaction from diferrous MauG to quinone MADH (Scheme 1). This reaction is thermodynamically favorable and does not require formation of a *bis*-Fe(IV) state, as do the TTQ biosynthetic reactions. In this reaction native MauG exhibits saturation behavior and a limiting first-order rate constant of 0.07 s^{-1} and K_d for complex formation with MADH of $10.1\text{ }\mu\text{M}$ (24). Ca^{2+} -depleted MauG did exhibit activity in this reaction. However, in this case the observed rate exhibited a linear dependence on quinone MADH concentration (Figure 5) and a bimolecular rate constant of $(6.8 \pm 0.4) \times 10^2\text{ M}^{-1}\text{s}^{-1}$ suggesting that formation of the protein-protein complex is the rate-limiting step. As the site of interaction with MADH is $19.4\text{ }\text{\AA}$ from the nearest heme iron of MauG (11), this result suggests that the presence or absence of Ca^{2+} exerts an effect on the global conformation of MauG.

Kinetic and equilibrium analysis of Ca^{2+} binding to Ca^{2+} -depleted MauG

Addition of CaCl_2 to Ca^{2+} -depleted MauG results in a change in the absorption spectrum back to that characteristic of native diferric MauG (Figure 6A). To determine the kinetic mechanism and kinetic parameters for Ca^{2+} binding, Ca^{2+} -depleted MauG was mixed with varied concentrations of CaCl_2 and the rate of the spectral change was monitored. Saturation

behavior was observed (Figure 6B) and a two-step mechanism was required to explain the data (eqs 1 and 2). This yielded a limiting first-order rate constant (k_3) of $(1.4 \pm 0.1) \times 10^{-3} \text{ s}^{-1}$ and a $K_d(1/K_d)$ value of $22.4 \pm 7.9 \text{ } \mu\text{M}$. The requirement for a two-step mechanism for Ca^{2+} binding is significant and the most likely explanation is that the absorbance change is a consequence of a relatively slow conformational change that is triggered by Ca^{2+} binding. The equilibrium binding of Ca^{2+} to Ca^{2+} -depleted MauG was also analyzed (Figure 6C) and the fit of the data to eq 3 yielded an equilibrium dissociation constant ($K_{d,eq}$) of $5.3 \pm 0.3 \text{ } \mu\text{M}$. The discrepancy between the kinetically-determined K_d value and that obtained by equilibrium binding reflect the fact that the binding event is not a simple single step mechanism but a two-step process. The kinetically-determined K_d value of $22.4 \text{ } \mu\text{M}$ describes the reversible binding of Ca^{2+} to Ca^{2+} -depleted MauG. The $K_{d,eq}$ value of $5.3 \text{ } \mu\text{M}$ is the concentration at which 50% of the protein has bound Ca^{2+} under equilibrium conditions. As this process involves two consecutive reversible steps (see eq 1), the overall equilibrium binding constant will be a product of the equilibrium constants for each of the two steps (eq 5) expressed either in terms of an equilibrium dissociation constant $K_{d,eq}$ or an

$$K_{d,eq} = K_d(k_4/k_3) \quad \text{or} \quad K_{a,eq} = K_a(k_3/k_4) \quad (5)$$

equilibrium association constant $K_{a,eq}$. Given the experimentally determined values of $K_d = 22.4 \text{ } \mu\text{M}$ and $K_{d,eq} = 5.3 \text{ } \mu\text{M}$, one can calculate the equilibrium constant that describes the relatively slow conformational change that follows binding to be $K_{eq} = k_3/k_4 = 4.2$. Thus, while relatively slow, this conformational change is highly favorable.

Protein secondary structure

To examine the structural changes caused by Ca^{2+} depletion of MauG, the CD spectra of both native and Ca^{2+} -depleted MauG were obtained under identical conditions. Figure 7 shows that these spectra are nearly identical, suggesting that there was not a significant change in secondary structure. Thus, the depletion of Ca^{2+} from MauG must cause loop or domain movements rather than more extensive protein unfolding.

Discussion

A common feature of several peroxidases is the presence of bound Ca^{2+} in the proximity of the heme(s). This is seen in both monoheme peroxidases with *b*-type hemes and in diheme peroxidases possessing *c*-type hemes. With the monoheme peroxidases the Ca^{2+} is strongly bound and does not dissociate under conditions in which the protein remains folded. For BCCP, which contains two *c*-type hemes, Ca^{2+} can dissociate in the absence of chelators resulting in an inactive enzyme under physiological conditions and in so doing regulates its activity. Ca^{2+} binding converts the enzyme from an inactive form to an active mixed-valence form (20,30). The observed spectroscopic changes upon reduction of the inactive diferric to the active mixed-valence state of BCCP are consistent with the structurally characterized loss of the distal His ligand at the H_2O_2 -binding heme (19–21). MauG possesses two *c*-type hemes and exhibits sequence and structural similarity to BCCPs, and the position and ligation of Ca^{2+} is identical (Figure 1) (11). However, diferric MauG already has an open distal site at the H_2O_2 -binding heme, which structurally makes it more aligned with the active mixed-valence state of BCCP. Interestingly, the *Nitrosomonas europaea* BCCP, which of the characterized BCCPs has the most sequence identity to MauG (28%), is active in both the diferric and mixed-valence states (31). Unlike the crystal structures of other diferric BCCPs, the *N. europaea* diferric BCCP has an open distal site for H_2O_2 -binding analogous to MauG (13). Thus, this BCCP may represent an evolutionary link between BCCPs and MauG.

The Ca^{2+} -binding site in MauG is located between the two hemes, and close to Trp93 (Figure 1A). A similarly placed Trp is present in the BCCP structures and has been suggested to mediate electron transfer between hemes in that class of enzyme (32). The orientations of the two hemes, Trp93 and Ca^{2+} with respect to each other are essentially the same in the MauG and BCCP structures. In MauG, Ca^{2+} is coordinated to four water molecules, the main-chain carbonyl oxygen atoms of Thr275 and Pro277 and the oxygen of the Asn66 side-chain forming a distorted pentagonal bipyramidal geometry (Figure 1B), which is identical to that observed in BCCP. The propionate A carboxylate oxygens of the six-coordinate His-Tyr ligated heme are hydrogen bonded to two of the waters that provide Ca^{2+} ligands, and this feature is invariant in all crystal structures of BCCPs and MauG (Figure 1B) (13, 19–21, 32, 33). This interaction has been postulated to modulate the pK_a of the heme propionate A of BCCP such that it remains deprotonated (20). The Ca^{2+} coordination sphere is unusual in having no carboxylate ligands from Asp or Glu residues, and this might also contribute to the propionate pK_a . In the proposed redox-coupled Bohr effect mechanism for BCCP only propionate D of the six-coordinate His-Met ligated heme (analogous to His-Tyr in MauG) is capable of taking up a proton upon reduction. This leads to the breakage of a hydrogen bond to a main-chain amide that propagates large conformational changes resulting in the dissociation of the distal His of the H_2O_2 -binding heme (20, 21). However in oxidized MauG and *N. europaea* BCCP there is no distal His present at this heme, and they adopt the propionate D conformer of the mixed-valence state of other BCCPs and consequently are catalytically competent in the diferric state (11, 13). It is noteworthy that both hemes of MauG are linked to the Ca^{2+} via hydrogen bonded waters (Figure 1B), since removal of Ca^{2+} from MauG causes alterations in the properties of both hemes.

The results of this study demonstrate that Ca^{2+} -dependent conformational changes in MauG affect its spectroscopic properties, and that the bound- Ca^{2+} is critical for the unusual catalytic properties of MauG. This indicates that the environment and conformation of the high-spin heme is significantly altered when Ca^{2+} is removed from MauG. These changes are reversible and consequently not the result of damage to the protein during the Ca^{2+} removal protocol. While inactive in the TTQ biosynthetic reactions which require the *bis*-Fe(IV) redox state, Ca^{2+} -depleted MauG was still redox active and able to transfer electrons to quinone MADH in a previously characterized non-biosynthetic reaction (24). Whereas the kinetics of this reaction with native MauG exhibit saturation behavior, the reaction with Ca^{2+} -depleted MauG exhibited a linear dependence on quinone MADH concentration. This indicates that after Ca^{2+} depletion, formation of the protein-protein complex is the rate-limiting step. This is consistent with the result suggesting a Ca^{2+} -dependent change in protein conformation. In this case, the Ca^{2+} depletion seems to have affected the MADH-binding site which is located $> 30 \text{ \AA}$ from the H_2O_2 -binding heme (11), suggesting that the structural influence of bound Ca^{2+} is propagated over a long distance through the protein. A Ca^{2+} -induced conformational change is additionally indicated by the results of the kinetic and equilibrium studies of Ca^{2+} binding to the Ca^{2+} -depleted MauG. The observed saturation behavior in the kinetic studies (hyperbolic concentration dependence of rate) requires a two-step mechanism for Ca^{2+} binding to Ca^{2+} -depleted MauG in which initially Ca^{2+} reversibly binds to Ca^{2+} -depleted MauG followed by a relatively slow but highly favorable conformational change that prevents the Ca^{2+} from readily dissociating. This conformational change is also reversible, but dissociation of Ca^{2+} can only occur from the unfavorable conformation which explains why prolonged incubation with a strong chelator is required to remove it from MauG.

The precise nature of the conformational change in MauG which is caused by removal of Ca^{2+} is not known, but the CD spectra are consistent with retention of the native protein secondary structure, indicating that significant protein unfolding is not occurring upon Ca^{2+}

depletion. The observation that only low-spin hemes are observed in the resonance Raman spectrum of Ca^{2+} -depleted MauG suggests that an amino acid residue has moved to enable it to provide a distal ligand to the heme which is five-coordinate in native MauG. The more planar structure of the heme macrocycle evidenced in these data is also consistent with a change in coordination and could be a consequence of an easing of constraints on the porphyrin ring. Resonance Raman studies of Ca^{2+} binding to both the oxidized and mixed-valence states of BCCP from *Paracoccus pantotrophus* also suggested that upon Ca^{2+} -depletion there was conversion of the five-coordinate high-spin heme to a six-coordinate low-spin heme (29,30). In BCCPs the residue which provides this removable distal ligand is a His. The conformation of the structural loop in the four crystal structures of BCCPs with dissociated His is very similar to that observed in MauG (11,13,19,21). However, in contrast to the BCCPs, the MauG loop does not contain a His, with Asp57 found at this position. Additional Asp, Glu and Met residues are located within 10 Å of the heme Fe in the native MauG structure, and so the identification of the sixth heme ligand is not known. Thus far it has not been possible to crystallize the Ca^{2+} -depleted MauG, and further spectroscopic and structural studies are in progress to try to identify the residue which provides the distal ligand in Ca^{2+} -depleted MauG and the nature of the accompanying structural change.

While calcium plays several critical functions in nature, its role in peroxidase function has received relatively little attention, with the BCCP being the best-characterized (discussed earlier). It is clear that tightly-bound Ca^{2+} is critical for the activity of a variety of other peroxidases. Horseradish peroxidase binds two Ca^{2+} which are required to maintain the structural integrity of the heme, for which the geometry for catalysis is lost upon Ca^{2+} removal (5,6). In cationic peanut peroxidase Ca^{2+} is believed to position a catalytically important amino acid around the heme group which also affects the orientation of the porphyrin ring (7). For manganese peroxidase and lignin peroxidase it has been demonstrated that thermal inactivation which causes distinct alterations in the heme environment, change in heme spin-state and changes in overall protein structure, is prevented and reversed in the presence of Ca^{2+} (8,9). In contrast to the peroxidases, heme-dependent oxygenases and oxidases do not typically contain bound Ca^{2+} . While the Ca^{2+} -binding sites of the monoheme and diheme peroxidases are different, the common feature of Ca^{2+} suggests that its role is specific to reaction of the heme with peroxide rather than a role in binding and activating molecular oxygen. MauG does not function primarily as a peroxidase, but can use H_2O_2 to catalyze posttranslational modifications of its protein substrate. This suggests that MauG may have originally been a peroxidase and then evolved to acquire its new function. The findings reported here expand the scope of heme-dependent enzymes in which Ca^{2+} plays an important role.

Acknowledgments

We thank Yu Tang for technical assistance.

This work was supported by NSF Grant MCB-0843537 (A.L.), NIH grants GM-41574 (V.L.D.), RCMI G12RR13459 (H.T.), GM-66569 (C.M.W.) and Minnesota Partnership for Biotechnology and Medical Genomics grant SPAP-05-0013-P-FY06 (C.M.W.).

References

1. Gagne SM, Tsuda S, Li MX, Smillie LB, Sykes BD. Structures of the troponin C regulatory domains in the apo and calcium-saturated states. *Nat Struct Biol.* 1995; 2:784–789. [PubMed: 7552750]
2. Tanaka T, Umekawa H, Saitoh M, Ishikawa T, Shin T, Ito M, Itoh H, Kawamatsu Y, Sugihara H, Hidaka H. Modulation of calmodulin function and of Ca^{2+} -induced smooth muscle contraction by the calmodulin antagonist, HT-74. *Mol Pharmacol.* 1986; 29:264–249. [PubMed: 3005834]

3. Murakami M, Kudo I. Phospholipase A₂. J Biochem. 2002; 131:285–292. [PubMed: 11872155]
4. Zeng J, Fenna RE. X-ray crystal structure of canine myeloperoxidase at 3 Å resolution. J Mol Biol. 1992; 226:185–207. [PubMed: 1320128]
5. Laberge M, Huang Q, Schweitzer-Stenner R, Fidy J. The endogenous calcium ions of horseradish peroxidase C are required to maintain the functional nonplanarity of the heme. Biophys J. 2003; 84:2542–2552. [PubMed: 12668462]
6. Howes BD, Feis A, Raimondi L, Indiani C, Smulevich G. The critical role of the proximal calcium ion in the structural properties of horseradish peroxidase. J Biol Chem. 2001; 276:40704–40711. [PubMed: 11546788]
7. Barber KR, Rodriguez Maranon MJ, Shaw GS, Van Huystee RB. Structural influence of calcium on the heme cavity of cationic peanut peroxidase as determined by 1H-NMR spectroscopy. Eur J Biochem. 1995; 232:825–833. [PubMed: 7588722]
8. Sutherland GR, Zapanta LS, Tien M, Aust SD. Role of calcium in maintaining the heme environment of manganese peroxidase. Biochemistry. 1997; 36:3654–3662. [PubMed: 9132018]
9. Poulos TL, Edwards SL, Wariishi H, Gold MH. Crystallographic refinement of lignin peroxidase at 2 Å. J Biol Chem. 1993; 268:4429–4440. [PubMed: 8440725]
10. Pettigrew GW, Echalié A, Pauleta SR. Structure and mechanism in the bacterial dihaem cytochrome *c* peroxidases. J Inorg Biochem. 2006; 100:551–567. [PubMed: 16434100]
11. Jensen LM, Sanishvili R, Davidson VL, Wilmot CM. In crystallo posttranslational modification within a MauG/pre-methylamine dehydrogenase complex. Science. 2010; 327:1392–1394. [PubMed: 20223990]
12. Wang Y, Graichen ME, Liu A, Pearson AR, Wilmot CM, Davidson VL. MauG, a novel diheme protein required for tryptophan tryptophylquinone biogenesis. Biochemistry. 2003; 42:7318–7325. [PubMed: 12809487]
13. Shimizu H, Schuller DJ, Lanzilotta WN, Sundaramoorthy M, Arciero DM, Hooper AB, Poulos TL. Crystal structure of *Nitrosomonas europaea* cytochrome *c* peroxidase and the structural basis for ligand switching in bacterial di-heme peroxidases. Biochemistry. 2001; 40:13483–13490. [PubMed: 11695895]
14. Li X, Jones LH, Pearson AR, Wilmot CM, Davidson VL. Mechanistic possibilities in MauG-dependent tryptophan tryptophylquinone biosynthesis. Biochemistry. 2006; 45:13276–13283. [PubMed: 17073448]
15. Li X, Feng M, Wang Y, Tachikawa H, Davidson VL. Evidence for redox cooperativity between α -type hemes of MauG which is likely coupled to oxygen activation during tryptophan tryptophylquinone biosynthesis. Biochemistry. 2006; 45:821–828. [PubMed: 16411758]
16. Davidson VL. Protein-derived cofactors. Expanding the scope of post-translational modifications. Biochemistry. 2007; 46:5283–5292. [PubMed: 17439161]
17. McIntire WS, Wemmer DE, Chistoserdov A, Lidstrom ME. A new cofactor in a prokaryotic enzyme: Tryptophan tryptophylquinone as the redox prosthetic group in methylamine dehydrogenase. Science. 1991; 252:817–824. [PubMed: 2028257]
18. Li X, Fu R, Lee S, Krebs C, Davidson VL, Liu A. A catalytic di-heme bis-Fe(IV) intermediate, alternative to an Fe(IV)=O porphyrin radical. Proc Natl Acad Sci USA. 2008; 105:8597–8600. [PubMed: 18562294]
19. Fulop V, Ridout CJ, Greenwood C, Hajdu J. Crystal structure of the di-haem cytochrome *c* peroxidase from *Pseudomonas aeruginosa*. Structure. 1995; 3:1225–1233. [PubMed: 8591033]
20. Echalié A, Brittain T, Wright J, Boycheva S, Mortuza GB, Fulop V, Watmough NJ. Redox-linked structural changes associated with the formation of a catalytically competent form of the diheme cytochrome *c* peroxidase from *Pseudomonas aeruginosa*. Biochemistry. 2008; 47:1947–1956. [PubMed: 18217775]
21. Echalié A, Goodhew CF, Pettigrew GW, Fulop V. Activation and catalysis of the di-heme cytochrome *c* peroxidase from *Paracoccus pantotrophus*. Structure. 2006; 14:107–117. [PubMed: 16407070]
22. Davidson VL. Methylamine dehydrogenases from methylotrophic bacteria. Methods Enzymol. 1990; 188:241–246. [PubMed: 2126329]

23. Pearson AR, De La Mora-Rey T, Graichen ME, Wang Y, Jones LH, Marimanikkupam S, Agger SA, Grimsrud PA, Davidson VL, Wilmot CM. Further insights into quinone cofactor biogenesis: Probing the role of MauG in methylamine dehydrogenase tryptophan tryptophylquinone formation. *Biochemistry*. 2004; 43:5494–5502. [PubMed: 15122915]
24. Shin S, Abu Tarboush N, Davidson VL. Long-range electron transfer reactions between hemes of MauG and different forms of tryptophan tryptophylquinone of methylamine dehydrogenase. *Biochemistry*. 2010; 49:5810–5816. [PubMed: 20540536]
25. Lee S, Shin S, Li X, Davidson V. Kinetic mechanism for the initial steps in MauG-dependent tryptophan tryptophylquinone biosynthesis. *Biochemistry*. 2009; 48:2442–2447. [PubMed: 19196017]
26. Hu S, Morris IK, Singh JP, Smith KM, Spiro TG. Complete assignment of cytochrome *c* resonance Raman spectra via enzymatic reconstitution with isotopically labeled heme. *J Am Chem Soc*. 1993; 115:12446–12458.
27. Tu, AT. Raman spectroscopy in biology; principles and applications. John Wiley and Sons Inc; New York: 1982. p. 331–337.
28. Desbois A. Resonance Raman spectroscopy of *c*-type cytochromes. *Biochimie*. 1994; 76:693–707. [PubMed: 7893820]
29. Pauleta SR, Lu Y, Goodhew CF, Moura I, Pettigrew GW, Shelnutt JA. Calcium-dependent conformation of a heme and fingerprint peptide of the diheme cytochrome *c* peroxidase from *Paracoccus pantotrophus*. *Biochemistry*. 2001; 40:6570–6579. [PubMed: 11380251]
30. Pauleta SR, Lu Y, Goodhew CF, Moura I, Pettigrew GW, Shelnutt JA. Calcium-dependent heme structure in the reduced forms of the bacterial cytochrome *c* peroxidase from *Paracoccus pantotrophus*. *Biochemistry*. 2008; 47:5841–5850. [PubMed: 18442258]
31. Arciero DM, Hooper AB. A di-heme cytochrome *c* peroxidase from *Nitrosomonas europaea* catalytically active in both the oxidized and half-reduced states. *J Biol Chem*. 1994; 269:11878–11886. [PubMed: 8163487]
32. De Smet L, Savvides SN, Van Horen E, Pettigrew G, Van Beeumen JJ. Structural and mutagenesis studies on the cytochrome *c* peroxidase from *Rhodobacter capsulatus* provide new insights into structure-function relationships of bacterial di-heme peroxidases. *J Biol Chem*. 2006; 281:4371–4379. [PubMed: 16314410]
33. Dias JM, Alves T, Bonifacio C, Pereira AS, Trincao J, Bourgeois D, Moura I, Romao MJ. Structural basis for the mechanism of Ca²⁺ activation of the di-heme cytochrome *c* peroxidase from *Pseudomonas nautica* 617. *Structure*. 2004; 12:961–973. [PubMed: 15274917]

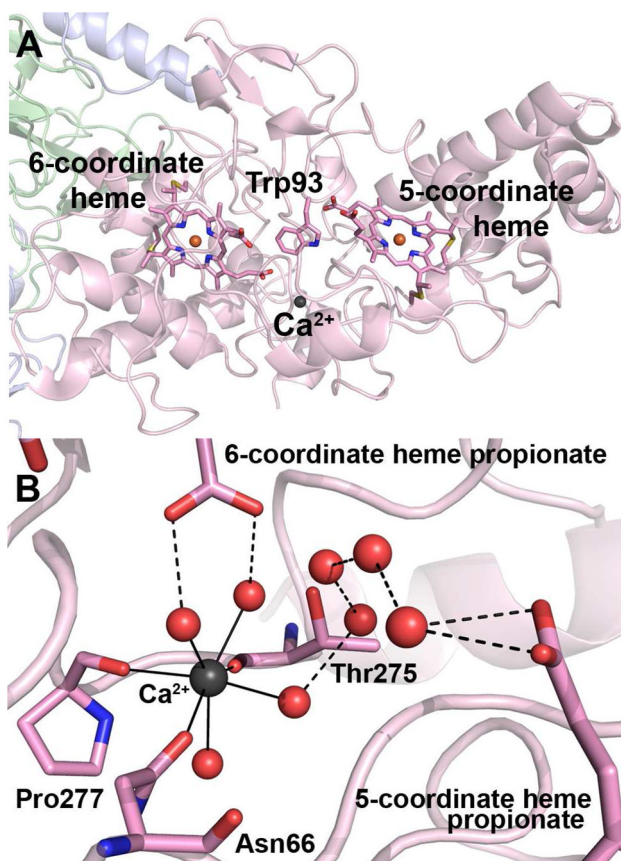


Figure 1.

Structure of the Ca^{2+} site in MauG. (A) Secondary structure depiction of MauG in complex with preMADH. (B) Ca^{2+} ligation with closest heme contacts and mediating water networks. Color scheme is MauG (pink); preMADH α (blue) and β (green). The hemes, Trp93 and Ca^{2+} ligands of MauG are drawn explicitly in stick representation colored by atom. Ca^{2+} , iron and water are represented by spheres colored black, orange and red respectively. Ca^{2+} -ligand bonds are represented as solid lines, and hydrogen bonds as dashed lines. This figure was produced using PyMOL (<http://www.pymol.org/>) and Protein Data Bank entry 3L4M.

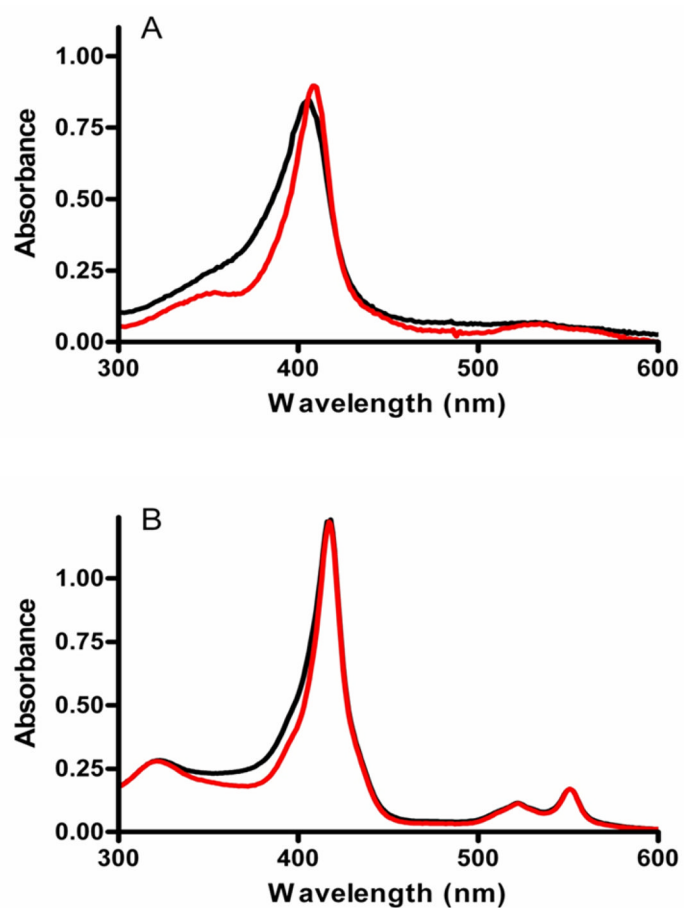


Figure 2. Effect of Ca^{2+} depletion on the absorption spectra of MauG. A. Overlay of the absorption spectra of diferric native (black) and diferric Ca^{2+} -depleted (red) MauG. B. Overlay of the absorption spectra of diferrous native (black) and diferrous Ca^{2+} -depleted (red) MauG.

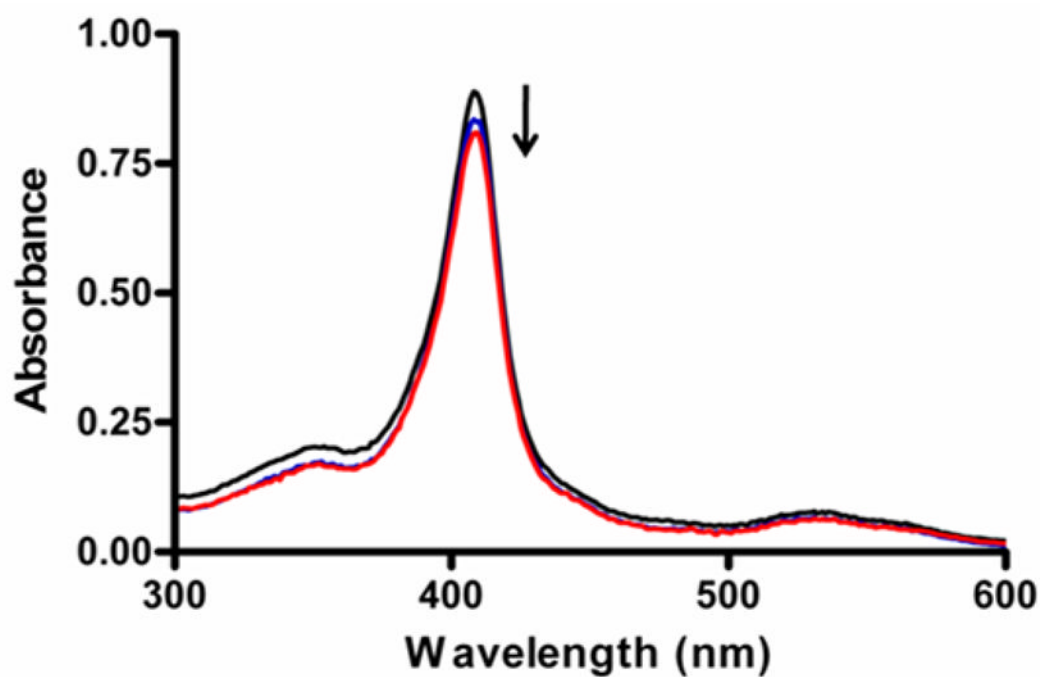


Figure 3. Changes in the absorption spectrum of Ca^{2+} -depleted MauG upon addition of H_2O_2 . Spectra were obtained before (black), immediately after addition of an equivalent of H_2O_2 (blue) and 10 min after addition of H_2O_2 (red) to Ca^{2+} -depleted MauG.

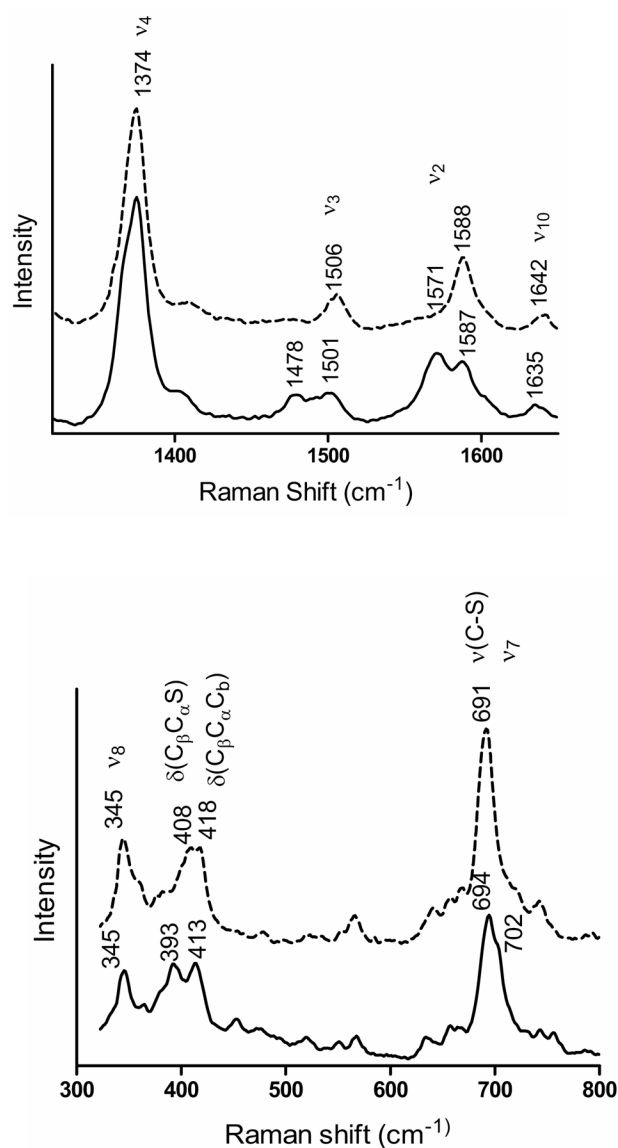


Figure 4. Effect of Ca^{2+} depletion on the resonance Raman spectrum of MauG. Overlay of the spectra of diferric native MauG (solid line) and Ca^{2+} -depleted MauG (dashed line) in the high frequency (top panel) and low frequency (bottom panel) regions. Relevant marker bands and their frequencies are indicated.

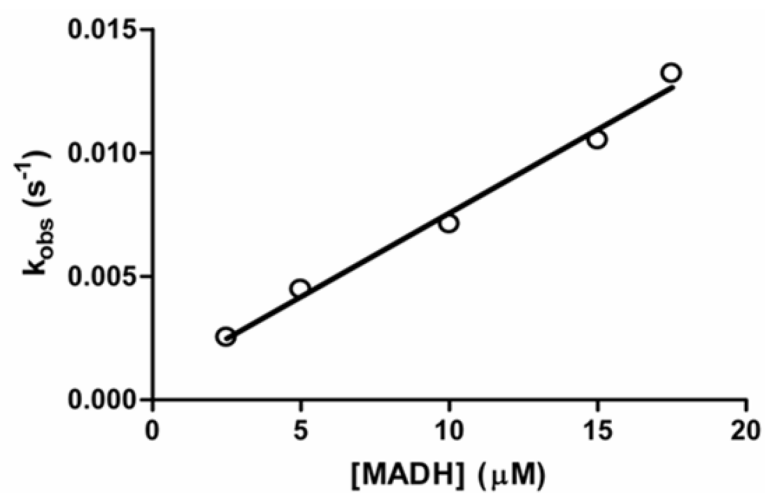


Figure 5. Concentration dependence of the rate of reaction of quinone MADH with diferrous Ca²⁺-depleted MauG. The line shows the linear regression fit of the data.

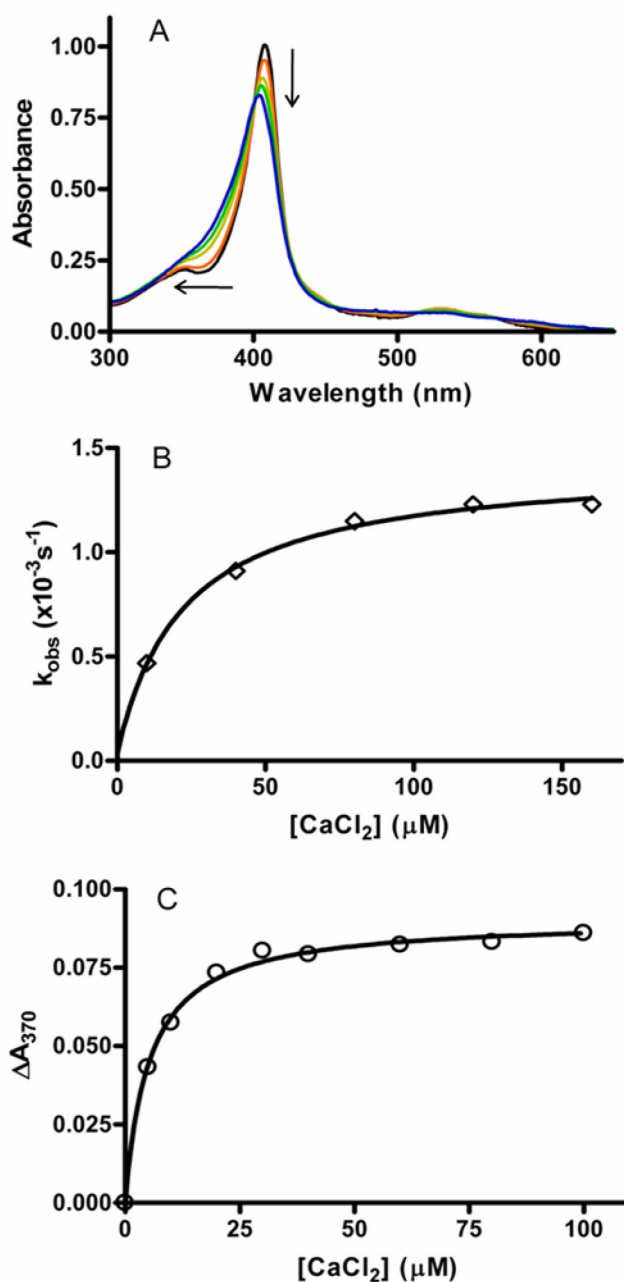


Figure 6. Binding of Ca^{2+} to Ca^{2+} -depleted MauG. A. Changes in the absorption spectrum of Ca^{2+} -depleted MauG after addition of 0.5 mM CaCl_2 . The spectra were recorded every 2 min after adding CaCl_2 . The arrows show the direction of the absorbance changes. B. Kinetic analysis of Ca^{2+} binding. Ca^{2+} -depleted MauG was mixed with varied concentrations of CaCl_2 and the rate of the spectral change was monitored. The line is a fit of the data to eq 2. C. Equilibrium binding of Ca^{2+} to Ca^{2+} -depleted MauG. CaCl_2 was added to Ca^{2+} -depleted MauG in increasing concentrations and the magnitude of the Ca^{2+} -induced spectral change was recorded after the system had reached equilibrium. The line is a fit of the data to eq 3.

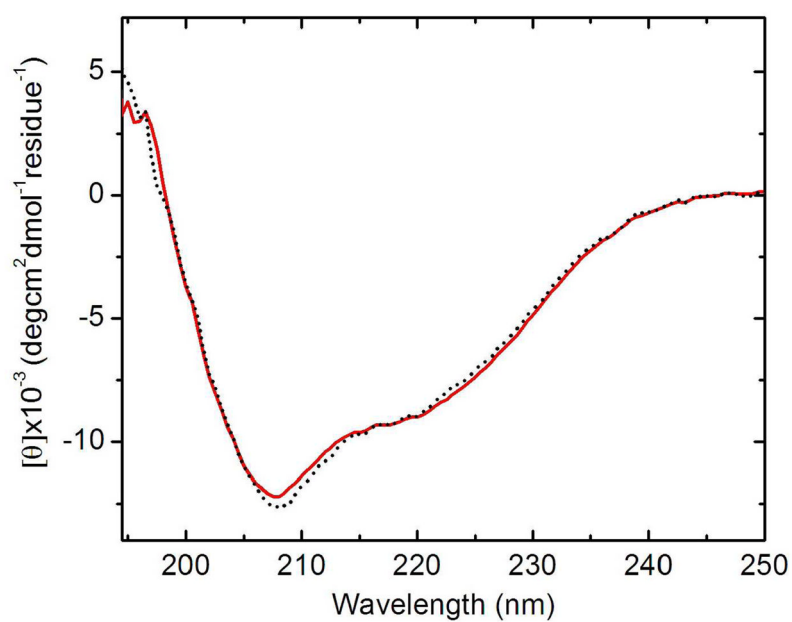
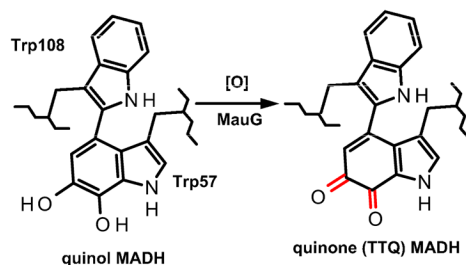
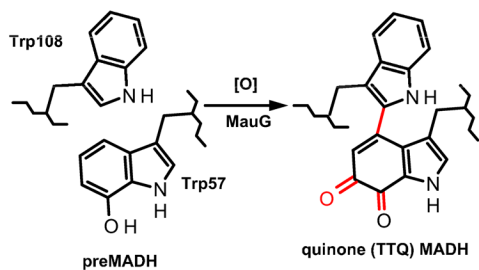
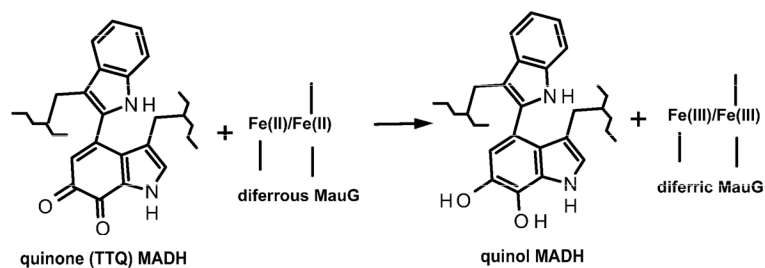


Figure 7. Effect of Ca^{2+} depletion on the circular dichroism spectrum of MauG. CD spectra of native (dotted black trace) and Ca^{2+} -depleted (solid red trace) MauG were recorded in 0.05 M potassium phosphate, pH 7.5.

STEADY STATE BIOSYNTHETIC REACTIONS



ELECTRON TRANSFER REACTION



Scheme 1.
Reactions catalyzed by MauG.